A Three-Dimensional Inverse Finite Element Analysis of the Heel Pad

Snehal Chokhandre

Jason P. Halloran

Department of Biomedical Engineering,
Cleveland Clinic,
Cleveland, OH 44195;
Computational Biomodeling (CoBi) Core,
Lerner Research Institute,
Cleveland Clinic,
Cleveland, OH 44195

Antonie J. van den Bogert

Orchard Kinetics LLC,
Cleveland, OH 44106

Ahmet Erdemir[1]

Department of Biomedical Engineering,
Cleveland Clinic,
Cleveland, OH 44195;
Computational Biomodeling (CoBi) Core,
Lerner Research Institute,
Cleveland Clinic,
Cleveland, OH 44195,
e-mail: erdemira@ccf.org

*Quantification of plantar tissue behavior of the heel pad is essential in developing computational models for predictive analysis of preventive treatment options such as footwear for patients with diabetes. Simulation based studies in the past have generally adopted heel pad properties from the literature, in return using heel-specific geometry with material properties of a different heel. In exceptional cases, patient-specific material characterization was performed with simplified two-dimensional models, without further evaluation of a heel-specific response under different loading conditions. The aim of this study was to conduct an inverse finite element analysis of the heel in order to calculate heel-specific material properties in situ. Multidimensional experimental data available from a previous cadaver study by Erdemir et al. ("An Elaborate Data Set Characterizing the Mechanical Response of the Foot," ASME J. Biomech. Eng., **131**(9), pp. 094502) was used for model development, optimization, and evaluation of material properties. A specimen-specific three-dimensional finite element representation was developed. Heel pad material properties were determined using inverse finite element analysis by fitting the model behavior to the experimental data. Compression dominant loading, applied using a spherical indenter, was used for optimization of the material properties. The optimized material properties were evaluated through simulations representative of a combined loading scenario (compression and anterior-posterior shear) with a spherical indenter and also of a compression dominant loading applied using an elevated platform. Optimized heel pad material coefficients were 0.001084 MPa (μ), 9.780 (α) (with an effective Poisson's ratio (ν) of 0.475), for a first-order nearly incompressible Ogden material model. The model predicted structural response of the heel pad was in good agreement for both the optimization (<1.05% maximum tool force, 0.9% maximum tool displacement) and validation cases (6.5% maximum tool force, 15% maximum tool displacement). The inverse analysis successfully predicted the material properties for the given specimen-specific heel pad using the experimental data for the specimen. The modeling framework and results can be used for accurate predictions of the three-dimensional interaction of the heel pad with its surroundings.* [DOI: 10.1115/1.4005692]

Keywords: Heel pad, plantar tissue, three-dimensional model, inverse finite element analysis, optimization

1 Introduction

The plantar tissue under the heel aids in the distribution of contact loads and provides shock absorption during locomotion [1,2]. The heel region is commonly associated with pain [3], and is known for risk of pressure ulcers [4,5] and diabetic foot ulcers [5]. Understanding heel pad mechanics is not only important for establishing the baseline for the healthy mechanical function of this structure, but it is also indispensable for the prescription of successful management strategies to accommodate mechanical dysfunction due to disease related changes. The mechanics of the heel relies on its geometry and the underlying tissue properties. Quantification of heel pad tissue behavior is therefore critical to understand normal and diseased tissue function and to design effective intervention strategies. Computational modeling has recently been utilized to explore healthy and pathological foot mechanics and related interventions, with many investigations focusing on the heel pad. Specifically, finite element (FE) analysis of the foot and heel pad have been extensively used in insole and footwear design [6–9], to study internal stresses [10], and to evaluate plantar pressure distribution [7], a mechanical variable commonly associated with diabetic foot ulceration or pressure ulcers at the heel [5]. Most models of the foot or heel pad have adopted literature based plantar tissue properties [7–9]. Only a handful of studies have associated the experimental data with model results [11,12].

The success of simulations based on finite element analysis relies on the accurate representation of specimen-specific geometry and specimen-specific tissue material properties, particularly in pathological conditions, such as diabetes. In addition, the investigations are ideally validated with controlled experimental data and are applicable to a wide range of physiologically relevant loading conditions. While acquisition of anatomical data to reconstruct realistic geometry is rather straightforward through well-established imaging modalities (magnetic resonance imaging, for example), identification of specimen-specific material properties, particularly in vivo and in situ, remains challenging. As mentioned before, many investigators relied on structural and material properties available in the literature obtained by others under a variety of testing conditions. Both in vivo and in vitro experimental studies have been performed to quantify the mechanical properties of the heel pad at structural and tissue levels. In vivo studies generally used indentation [13–16] or impact loading scenarios [17]. Typically performed to replicate heel strike dynamics, impact tests helped quantify force-deformation behavior at high loading rates and indentation tests quantified the response at low loading

[1]Corresponding author.

Contributed by the Bioengineering Division of ASME for publication in the JOURNAL OF BIOMECHANICAL ENGINEERING. Manuscript received October 14, 2011; final manuscript received January 3, 2012; accepted manuscript posted February 21, 2012; published online March 16, 2012. Assoc. Editor: Stephen Klisch.

rates. Without disassociation of geometric effects and boundary conditions, these studies only provide a description of the overall structural response, lacking the quantification of the real stress-strain response of the heel pad, which is necessary for finite element analysis. In vitro tests have also proved valuable and have been used to quantify compressive material properties of the fat pad [18] and plantar tissue [19]. These studies obtained the nonlinearly elastic and/or viscoelastic properties from mechanical testing of uniformly shaped isolated tissue samples obtained from cadaver specimens. Although such data are useful for finite element analysis, it does not address heel-specific modeling since the material properties are not necessarily that of the heel from which the geometry is reconstructed.

Identification of specimen-specific heel pad properties acquired through in situ testing has potential applications for the determination of material properties of the heel pad in vivo. This can lead towards personalized models of this structure that can be used for the development of patient-specific intervention strategies. Inverse finite element analysis can be used for this purpose. For example, in vivo indentation tests performed with concurrent acquisition of tissue thickness and coupled to an inverse modeling framework can yield stress-strain behavior. Erdemir et al. [11] illustrated the potential of inverse finite element analysis to obtain material properties of healthy and diabetic heel pads. Nonetheless, the simulations were limited to two-dimensions, with a simplified representation of the heel. In addition, the validity of the obtained parameters under complex three-dimensional loading modes has not been addressed.

The overall goal of this study was to develop a specimen-specific heel pad model capable of predicting a specimen-specific multiaxis (all three components of the load) response. To achieve this goal, and to illustrate the pipeline for in situ specimen-specific modeling, the specific aims were: (i) to optimize nonlinear elastic material properties of the heel pad using an inverse finite element analysis framework supported by specimen-specific compression dominant multiaxis load-deformation data obtained using a spherical indenter, and (ii) to validate the model against experimental data from a combined compression and shear test applied using a spherical indenter and from a compression dominant test conducted using an elevated flat platform.

2 Methods

2.1 Mechanical Testing Data. To obtain specimen specific heel pad material properties, mechanical testing and imaging data from a previous work was utilized [20]. In summary, the data set consists of comprehensive in situ multidimensional mechanical testing, which was performed on a whole cadaver foot from a 58-year old male donor. Only heel pad data was used in the present study. A spherical stainless steel indenter (25.4 mm in diameter) and an elevated flat platform (86 mm × 51 mm × 151 mm; width × height × length) were used to impart combinations of different types of loading. Three datasets were used in this study: compression dominant indentation, indentation with compression and shear, and compression with elevated platform. All of the tests were conducted on a six degree of freedom system (Rotopod, R2000, Parallel Robotic Systems Corp., Hampton, NH, USA). Kinematic measurement resolution of the robot was 0.001 mm for translations, 0.001 deg for rotations. Kinetic resolution of the spatial load transducer was 0.5 N (1.1 N for compression) and 0.07 Nm. During testing, the robot was first moved at a rate of 0.01 m/s up to desired reaction force magnitudes of 220 N (compression only) for the indenter, 220 N (compression), and 80 N (shear) for the indenter and 550 N (compression) for the elevated platform. The trajectories calculated by these experiments were utilized and tool positions were then prescribed using displacement control at a rate of 0.04 m/s, during which the corresponding reactions were recorded. The rate of 0.04 m/s was chosen to replicate lifelike loading rates on plantar tissue [21]. The multidimensional experimental reaction forces and moments were collected via a load cell (at 1000 Hz) and, along with the robot kinematics data (at 50 Hz), all measurements were transformed to the model coordinate system (described in the following text) before use in the FE model.

The data set also included computed tomography (CT–SOMATOM Sensation 64, Siemens Medical Solutions USA, Inc., Malven, PA, USA) scans, which were used to create an anatomically realistic geometric representation of the heel pad (for computational model development see Sec. 2.2). Image resolution was 512 × 512 pixels with a pixel size of 0.365 mm. The slice thickness was 1 mm. To establish registration between the mechanical testing data, the image set, and thus the computational model, a three-dimensional digitizer (Microscribe G2L, Immersion Corp, San Jose, CA, USA; 0.130 mm resolution, 0.430 mm accuracy) was used to collect spatial coordinates of four landmarks during the experimental testing. Points included the tip of the second toe, posterior aspect of the heel at the calcaneal tuberosity, medial aspect of the first metatarsal head, and the lateral aspect of the fifth metatarsal head. The landmarks established a "foot" coordinate system with the anterior-posterior direction defined approximately along the long axis of the foot (connecting the posterior aspect of the heel and the tip of the second toe). In the following, a dummy axis, approximately along the medial-lateral direction, was defined using the medial and lateral metatarsal points. The superior-inferior axis was defined as the cross product of the dummy axis and the anterior-posterior direction. To establish an orthogonal coordinate system, the medial-lateral direction was subsequently defined as the cross product of the anterior-posterior and superior-inferior directions. The location of the same anatomical landmarks on the image set allowed registration between the experimental coordinate systems and that of the model. However, since the specimen was not in the same position when it is digitized in the experimental setup and during imaging, the experimental coordinate system may not accurately match with the model coordinate system.

2.2 Finite Element Representation. A geometrically consistent finite element model of the cadaver foot was developed for the study. The boundaries of the bone and soft tissue were obtained from supplementary data submitted along with work by Erdemir et al. [20]. (see https://simtk.org/home/multidomain). The computed tomography images were segmented to define bone and soft tissue geometries using an in-house semi-automated software (Geomata, Computational Biomodeling Core, Cleveland Clinic, Cleveland, OH, USA). Segmentation points were loaded into an open source geometric design software, Salome (Open Cascade SAS, Euriware Group, Guyancourt, France) (http://www.salome-platform.org), and used to create three-dimensional geometric curves for each image slice in an automated fashion. Subsequently, whole foot and internal bone surface geometries were generated using Rhinoceros 4.0 (McNeel North America, Seattle, WA, USA) (see Fig. 1). For the calcaneus and talus for example, this process resulted in root-mean-square errors in surface approximation of 0.99 mm and 1.23 mm, as calculated from the distance between the actual coordinates of the segmented points and the generated surface.

For this study, the rear foot region (heel) was isolated and two meshes, with 14,520 and 30,576 linear hexahedral elements of type C3D8H (8-node linear brick, hybrid with constant pressure [22]), were created using TrueGrid (XYZ Scientific Applications, Inc., Livermore, CA, USA) (see Fig. 1). Rear foot bones were lumped and the calcaneus, talus, and navicular bones were meshed as one entity. This was done to replicate the experimental conditions in which the calcaneus and talus were fixed relative to each other using a screw so that the heel pad material could be characterized without the influence of the talocalcaneal joint motion. Finite element analysis for each specific combination of tool and loading profile were performed using Abaqus/Standard (Version 6.7-1, Simulia, Providence, RI, USA). To determine the adequacy

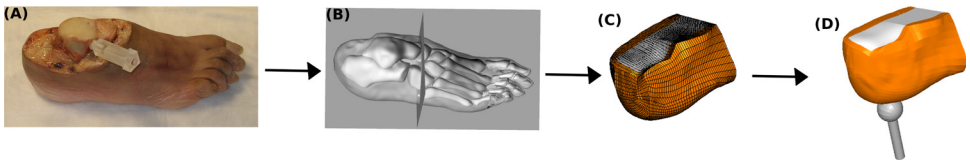

Fig. 1 Model development: (*a*) cadaver specimen for which the mechanical testing and imaging data was used in the finite element model development, (*b*) three-dimensional surface geometries created for the specimen with a plane illustrating the separation of the region of interest (heel), (*c*) hexahedral mesh of the heel, and (*d*) finite element model showing heel and indenter.

of the mesh, a preliminary analysis with sample indentation simulations, by approximately 50% of the initial heel pad thickness, were performed. The peak reaction load for the coarse mesh was 27.4 N and it was 30 N for the fine mesh. Owing to the difference in the peak force of less than 10%, a further increase in mesh density was deemed unnecessary and the fine mesh with 30,576 elements was used in the study. This mesh also appeared to have a well-behaving contact, as reflected by visually inspected stress contours. Note that while this mesh was adequate for modeling the structural response (force-displacement) of the heel (modeled variables in the inverse finite element analysis, see Sec. 2.3), a detailed mesh convergence study (with increased mesh densities) may be necessary, when plantar pressures and/or internal stresses are of interest.

The bones and the tools (indenter and elevated platform) were assumed to be rigid and the lumped heel-pad material (plantar soft tissue, including skin and fat) was represented as a nonlinearly elastic material with an effective Poisson's ratio (v) of 0.475, to approximate near incompressibility. A first order Ogden definition was used to define the strain energy function of the heel pad tissue [22]:

$$U = \left(2\frac{\mu}{\alpha^2}\right)\left(\lambda_1^{\alpha} + \lambda_2^{\alpha} + \lambda_3^{\alpha} - 3\right) + \frac{1}{D}(J-1)^2 \tag{1}$$

where λ_{1-3} are the deviatoric principle stretches. Coefficients μ, α, and D describe the nonlinear elastic response of the material, and are related to the initial shear modulus, strain hardening behavior, and the material compressibility, respectively. The parameter D is given as

$$D = \frac{2\mu(1+v)}{3(1-2v)} \tag{2}$$

2.3 Inverse Finite Element Analysis. The finite element representation previously outlined was utilized in an inverse fashion to obtain heel pad material properties that best reflect a specimen-specific structural response. Load-deformation data from the compression dominant spherical indenter test was used for the optimization of material properties (Fig. 2). In our inverse framework, the sum of squared differences between the model predicted forces and the measured experimental forces at each increment was minimized in order to obtain the specimen-specific material properties μ and α (Eq. (3)). Thirteen evenly spaced data points were defined to calculate the model versus experimental squared error metric

$$\text{Error} = \sum_{i=1}^{3}\sum_{k=1}^{13}\left(F_{ik}^{M} - F_{ik}^{E}\right)^2 \tag{3}$$

where F^M and F^E are model predicted and experimental forces, respectively, k are the data points, and i are the three anatomical reaction components. Initial guess values of 0.0001 MPa and 11, for μ and α, respectively, were defined and the Truncated Newton optimization algorithm available in SciPy (Enthought, Inc., Austin, TX, USA) (http://www.scipy.org) was used to iteratively solve the nonlinear least-squares minimization problem.

A hybrid control approach was used to apply the experimental loads to the model (Fig. 3). A linear spring (with a stiffness of k) placed between the reference point on the tool and a coincident point (control point) was used to drive the tool. The trajectory of the control point (d') in the FE model was calculated using the experimental forces and displacements (d^E), as opposed to directly driving the tool using the displacement data from the mechanical tests. This approach weakly prescribes the tool displacement and, within the inverse finite element analysis, concurrently minimizes the difference between model displacements (d^M) and experimental displacements (as opposed to forces only, as described by Eq. (3)). The forces in the spring are given by

$$F^E = k\left(d^E - d'\right) \tag{4}$$

The control point displacements are then calculated by

$$d' = d^E - \frac{F^E}{k} \tag{5}$$

The forces predicted by the model should be equal to the forces in the spring due to static equilibrium conditions

$$F^M = k\left(d^M - d'\right) \tag{6}$$

Substituting Eqs. (4) and (6) in Eq. (3) yields

$$\min\sum\left(F^M - F^E\right)^2 = \min\sum k^2\left(d^M - d^E\right)^2 \tag{7}$$

The spring stiffness k was chosen to be 10 N/mm for translations and rotations were fixed. Note that a pure displacement control is possible as k approaches infinity and a pure force control is possible as k approaches to zero, although the solution should be independent of this value. This facilitated a comparison of model and experimental force and displacement outputs and had the important benefit of accommodating experimental errors both in the force and displacement measurements along with aiding with model convergence, since neither displacements nor forces were directly prescribed to the tool. Large unrealistic element deformations, potentially a result of registration errors (between model coordinate system and that of the experiment), were prevented.

2.4 Validation. The optimized material properties were utilized to compare model results for two additional sets of experimental data: (i) combined loading of compression and shear applied by the spherical indenter, and (ii) compression dominant loading applied by the elevated flat platform (Fig. 2). Since viscous contributions were not modeled, tissue unloading curves were truncated from the comparison. For both validation data sets, the hybrid control setup was utilized (Fig. 2) and model predicted

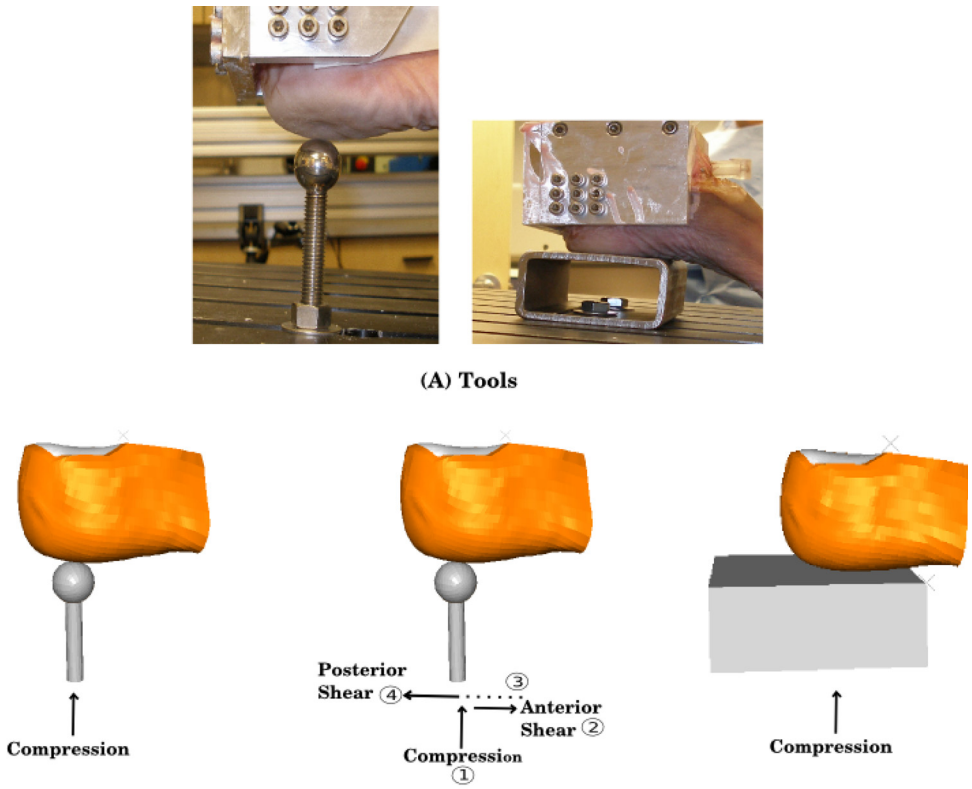

Fig. 2 Experimental load-tool combinations used for inverse finite element analysis and validation purposes: (*a*) tools—a spherical indenter (25.4 mm in diameter) and a flat elevated platform (86 mm × 51 mm × 151 mm; width × height × length), (*b*) compression dominant indentation conditions used for material properties optimization, and (*c*) combined loading of compression and anterior-posterior shear applied using the indenter and compression dominant loading applied using the flat elevated platform; both used for validation.

behavior was compared with the experimental reaction forces and displacements. The root-mean-square errors (RMSE), both in absolute units and normalized by maximum force or displacement of the trial, were calculated.

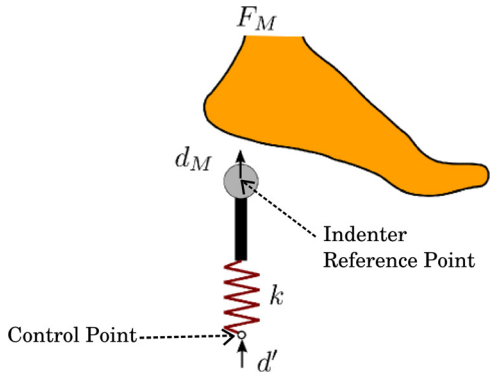

Fig. 3 A hybrid control was used to apply the experimental tool trajectory in the model, consisting of a spring component driving the tool (indenter or elevated platform). A control point was defined and a linear spring was attached between the control point and the indenter reference point. Displacements of the control point implicitly applied experimental forces (see text for details). In the model, the control point is defined at the same location as the indenter reference point and is shown separately in the figure for illustration purposes.

3 Results

The inverse FE analysis of indentation, utilizing compression dominant data, provided specimen-specific nonlinear elastic coefficients of the heel pad as: $\mu = 0.001084$ MPa and $\alpha = 9.780$. A total of 117 optimization iterations were required and an RMSE of 0.7136 N (0.61% max force magnitude) was obtained between model predicted and experimental compressive dominant force magnitudes (Table 1). The structural response (three-dimensional forces and displacements), as predicted by the model utilizing optimized coefficients, was in good agreement with experimental measurements (Fig. 4). As expected, for the data utilized for the inverse analysis, components of off-axis force predictions had an RMSE less than 1.5% of the maximum force magnitude (Table 1). All displacement RMSEs were less than 1% of the maximum displacement magnitude (Table 2).

The simulations also had the capacity to reproduce loading conditions for combined loading and when using a different tool; yet the RMSEs were higher than that of the data used for the inverse analysis. For the combined loading test (compression and shear with the indenter), the force RMSE was less than 7% of the maximum force magnitude (Table 1) and the displacement RMSE was less than 14% of the maximum displacement magnitude (Table 2) (also see Fig. 5). In the second validation scenario, compression dominant loading with a different tool (elevated platform), the force predictions had an RMSE less than 2% of the maximum force magnitude (Table 1). The displacement RMSEs were less than 6% of the maximum displacement magnitude. Both experimental and model predicted structural responses of the heel pad, when compressed using an elevated platform, can be seen in Fig. 6.

Table 1 Root mean square errors (RMSE) between model predicted and experimental forces for dominant and off-axis loading directions for all loading scenarios

Loading (tool)	Maximum force magnitude (N)	RMSE (N), as a percentage of maximum force magnitude		
		Superior-inferior	Medial-lateral	Anterior-posterior
Compression (indenter)	115.27	0.71, 0.61%	0.67, 0.58%	1.20, 1.04%
Compression-shear (indenter)	339.37	10.54, 3.1%	6.52, 1.92%	21.67, 6.44%
Compression (elevated platform)	274	4.1, 1.49%	2.6, 0.94%	5.5, 2.0%

4 Discussion

The study successfully resulted in the development of a three-dimensional heel pad model capable of predicting a specimen-specific multiaxial (all loading directions) response for compression along with shear dominant loading scenarios induced by different tools. An inverse FE approach was utilized to optimize the nonlinear elastic material properties based on indentation data obtained using a spherical indenter and compression dominant loading, similar to approaches previously utilized [11], yet has not been applied in a three-dimensional sense nor validated before. Unique to this study, the optimized material parameters were evaluated under two additional loading scenarios.

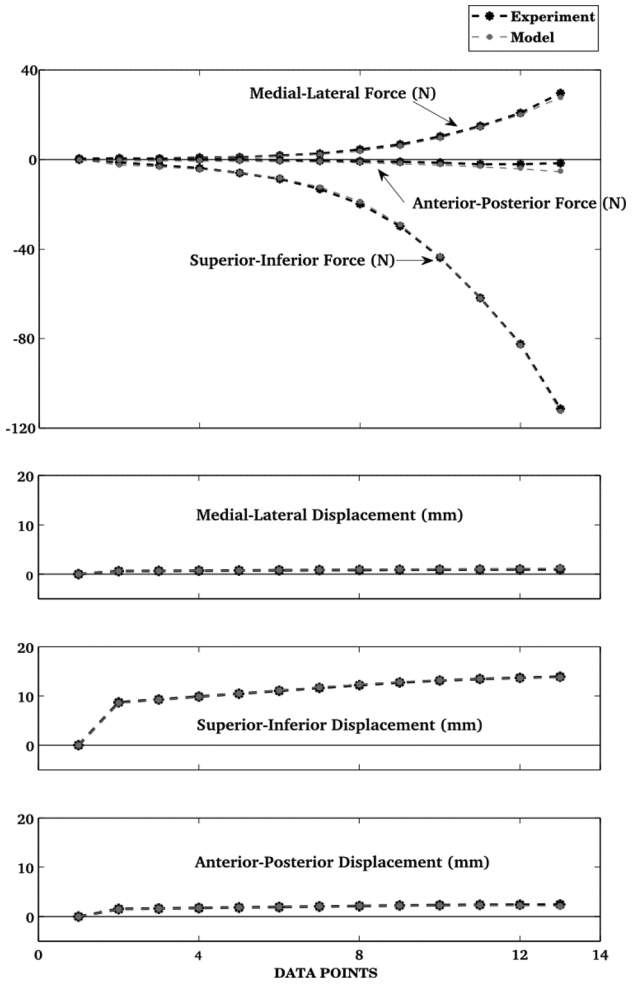

Fig. 4 Structural response (forces and displacements) of the heel pad under the compression dominant indentation data. Both experimental and model predicted values are shown. The data set was used for the inverse finite element analysis and the model predictions utilized the final optimized material coefficients.

The initial elastic modulus, as described by the Ogden material formulation, being 3μ [22], was 0.003252 MPa for this study. Both in vivo and in vitro studies have quantified heel-pad mechanical properties [11,15,18]. Hsu et al. [15] reported a value of 0.168 MPa, however, due to their determination of the modulus as the maximum stress divided by the maximum strain, it is speculated that their calculations resulted in relatively high modulus values. In a similar study, Gefen et al. [23] found 0.105 MPa as their initial modulus and over a 0.3 MPa tangential modulus at 30% compressive strain. At 30% strain, the tangential modulus from our calculations was 0.0154 MPa. Erdemir et al. [11], alternatively, utilized an Ogden strain energy function and found the initial elastic modulus to be approximately 0.050 MPa. When compared to our study, these in vivo studies all found higher stiffness values. These differences could be attributed to the chosen techniques, however, it is also evident that a wide range of potential values is possible, even if the results are constrained to in vivo studies. Previous in vitro results have also demonstrated variable elastic moduli. Miller-Young [18] reported a value of 0.00000012 MPa from an unconfined compression test performed on isolated fat pads. However, an unconfined compression test done on isolated full thickness plantar tissue samples by Pai and Ledoux [24] provided a value of 0.593 MPa. This high variability in reported values could be due to the differences in test methods, donor age, vascular condition, number of samples or subjects, and whether the study was conducted in vivo or in vitro. The α term, which is the rate of change in the tangential modulus with increasing strain (Eq. (1)), can only be compared to studies which utilized an Ogden material model. As an available plantar tissue comparison, Erdemir et al. [11] reported an α value of 6.82 ± 1.57, for which our 9.78 result for α falls within two standard deviations. For a more appropriate comparison, the tangential modulus for 30% of the compressive strain was calculated for their model: 0.9055 MPa, against 0.0154 MPa in our calculations.

A generally good agreement was achieved when optimized material coefficients were used in simulations that tried to reproduce different data sets than those utilized for the inverse analysis. Nonetheless, the anterior-posterior degree of freedom experienced a marked deviation between the model and experimental results. It is speculated that registration errors between the image set and the experimental setup, essentially due to the misalignment of the force transducer and the foot coordinate systems, may lead to the discrepancies found for this degree of freedom. A sensitivity study was performed to ascertain the effect of this misalignment, if any, on the observed deviations. Changes to the representation of the experimental forces were evaluated through ± 5 deg rotations (clockwise and counterclockwise) about the superior axis within the foot coordinate system. The anterior force changed up to 3.5 N, whereas the medial-lateral force component remained relatively consistent (Fig. 7). This indicates that a potential misalignment between the foot and load cell coordinate systems may explain some of the observed deviations. Additional sensitivity analysis will likely quantify sources of error specific to the relative coordinate frame alignment.

Multiaxis evaluation realized marked changes in the force response for the nondominant loading directions. Contrary to our

Table 2 Root mean square errors (RMSE) between model predicted experimental displacements for dominant and off-axis loading directions for all loading scenarios

		RMSE (mm), as a percentage of maximum displacement		
Loading (tool)	Maximum displacement magnitude (mm)	Superior-inferior	Medial-lateral	Anterior-posterior
Compression (indenter)	14	0.07, 0.5%	0.06, 0.4%	0.12, 0.85%
Compression-shear (indenter)	17.18	1, 5.8%	0.65, 3.78%	2.4, 14%
Compression (elevated platform)	10.25	0.41, 4%	0.26, 2.53%	0.55, 5.36%

anticipation, during the application of shear (anterior-posterior) with the spherical indenter, the medial-lateral force increased more predominantly than the anterior-posterior force (Fig. 5). It is speculated that the nonuniform geometry of the calcaneus, combined with the relatively incompressible plantar tissue, led to the observed deviations. As the indentation took place, the relative location of the indenter around the bony prominence, may result in compression of the nearly incompressible tissue and explains the off-axis (medio-lateral) reaction forces generated on the tool (Fig. 8). This result indicates that off-axis loading and three-dimensional representation of the foot-indenter interaction are important factors to consider during the quantification of plantar tissue mechanics. Furthermore, since the talocalcaneal joint was fixed, the overall stiffness of the structure might have increased, leading to high recorded forces.

A unique feature and contribution of the study was the adoption of a hybrid loading scheme (Eqs. (4)–(6)). Instead of a direct application of experimental boundary conditions (displacements or loads) to the tool of interest, displacements were applied via a spring. This weakly prescribed tool displacement allowed concurrent minimization of error between the model and experimentally

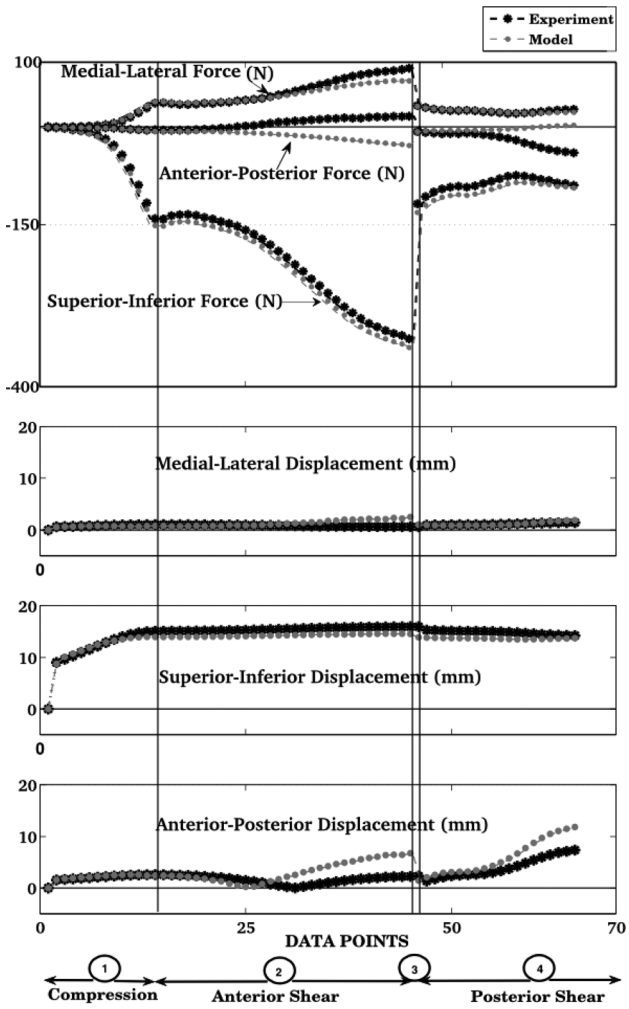

Fig. 5 Structural response of the heel under the combined loading of compression and anterior-posterior shear applied using a spherical indenter. Experimental forces and displacements are compared with the model predictions. The experimental data set was used for validation where the model predictions relied on optimized material coefficients obtained through another experimental data set (see Fig. 4). A compressive load application (1), was followed by an anterior shear (2), maintaining the approximate compressive displacement. The data for return of the tool to its original position (unloading) (3) was not considered in the analysis. Upon returning to the initial position, a posterior shear was applied (4).

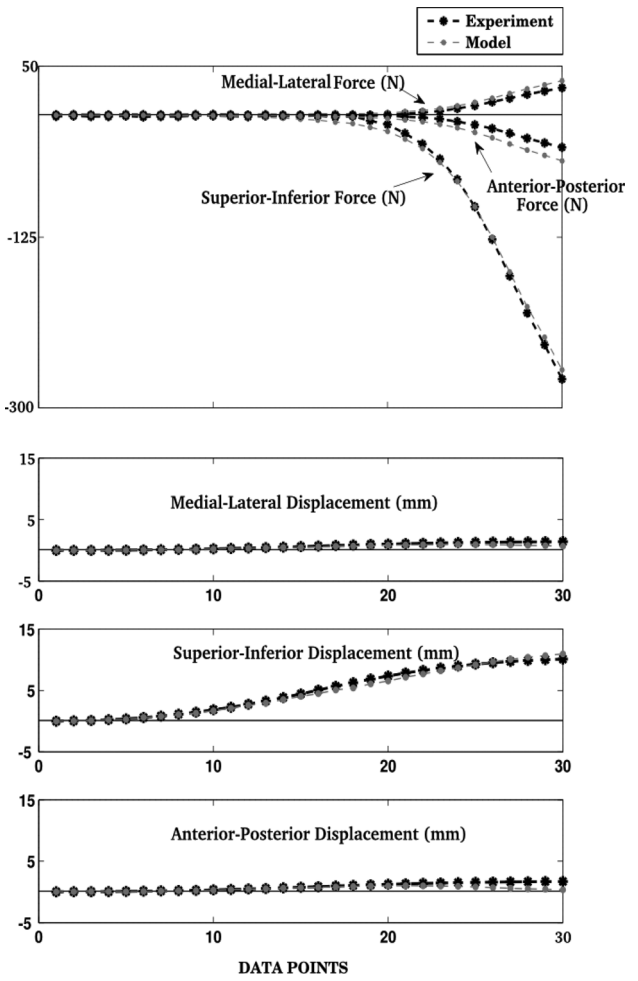

Fig. 6 Structural response of the heel under a compression dominant loading applied using an elevated platform. Experimental forces and displacements are compared with the model predictions.

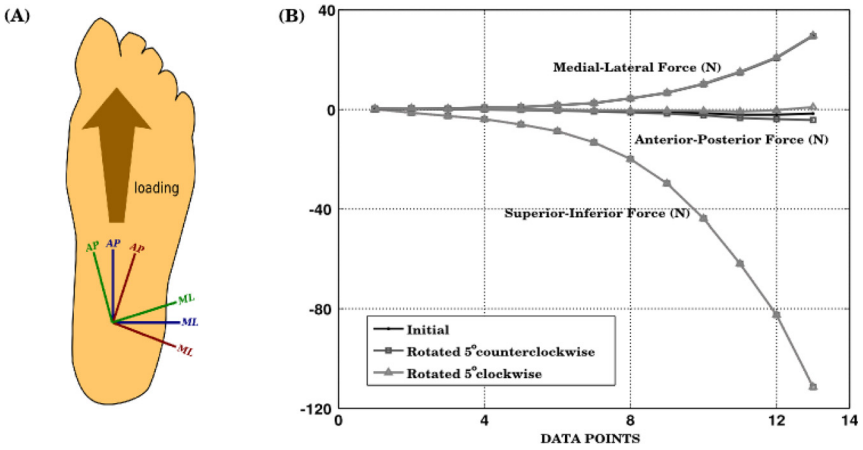

Fig. 7 Evaluation of the effect of misalignment between the foot and the load transducer coordinate systems on the force components. This sensitivity analysis was performed to assess the causes of deviations observed between the experimental force values and those predicted by the model, in particular, the anterior-posterior forces.

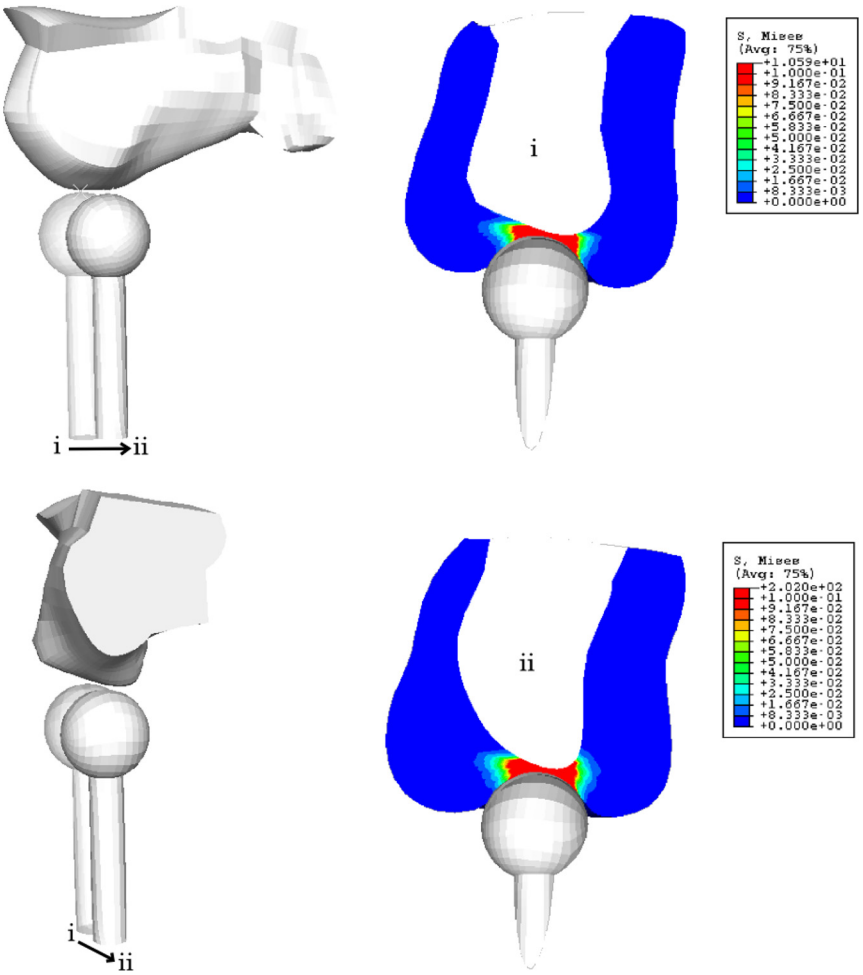

Fig. 8 As the indenter gets closer to the bony landmark (from position (i) to position (ii)), internal loading of the heel (as illustrated by the von Mises stress distribution) may cause large off-axis forces that may not necessarily align with the direction of the tool movement. Note that the dominant shear displacement (anterior) is approximately perpendicular to the plane of the cut, where the mediolateral reaction force is higher in an unexpected fashion.

predicted forces along with measured and simulated indenter displacements, at least in part, accommodating for potential model to experiment registration errors. Due to computational limitations, i.e., convergence problems associated with large distortions in elements due to nonphysiological deformations, and/or potential registration errors, hybrid control of the tool displacement also aided a robust simulation process that is paramount for automated iterative investigations such as inverse finite element analysis. The fact that all FE simulations provided complete solutions during optimization may indicate the benefit of this approach.

As in any modeling study, this work also has inherent limitations that should be addressed in order to properly frame the results. The material representation of the heel pad structure was simplistic since the fat pad and skin were not separately modeled. Bulk material properties for the heel pad were found despite the natural geometry being made up of distinct tissue components. The potential to capture more complex behavior with a multilayered model is possible although bulk heel pad material definitions have been shown to accurately predict the contact behavior and force response [11]. Upcoming studies will likely address this level of complexity to understand plantar tissue mechanics in more detail [25]. Additionally, the loading rate used in this study was meant to represent a typical heel strike during gait, although rate dependent behavior, i.e., viscoelasticity, was not modeled. As such, these results are potentially limited to the chosen loading rates. While the study included only one specimen and the inclusion of additional samples is desirable, and will be performed, this specimen-specific approach demonstrated the potential to capture the complicated mechanical behavior of the heel. The ability of the nonlinearly elastic Ogden material definition to predict off-axis and simulated shear loads was noteworthy, even though parameter development was based on a compression dominant test. That being stated, the shear loading was applied along the long axis of the foot during approximated heel strike conditions and it is recognized that this loading will not account for all potential in vivo conditions. With regard to the optimization approach itself, a gradient based method has the potential to settle at a local minimum and sensitivity to the initial guess was not performed. From a practical perspective, the realized parameters achieved good model to experimental agreement, although a global minimum is not guaranteed. As the first study to implement this type of complex testing in conjunction with specimen-specific model development and validation, we feel that this is an acceptable starting point for future simulations and experiments.

Validated three-dimensional models of the heel pad are essential in simulation-based studies to understand healthy and pathological mechanics and are ideally suited for the development of treatment options. Our analysis illustrated that it is possible to capture the off-axis and simulated shear behavior, at least for the chosen loading conditions and tools. This modeling framework can be used to predict internal tissue mechanics, plantar pressure distribution, and includes the potential to assess harmful loading conditions, e.g., shear, a current concern in diabetic foot ulceration [26]. Given the availability of data [20], this study could also be extended to include forefoot passive response, effectively modeling the whole foot's structural behavior. Such models would be ideally suited for the study of insole and footwear design, including mechanical intervention strategies to address diseased tissue. Since the experimental data used in the study was collected in situ, the technique can also be potentially used in quantifying heel pad properties using patient specific data for developing personalized intervention strategies. To our knowledge, this study is the first to optimize nonlinear elastic material parameters using dominant and off-axis loads in a three-dimensional heel pad model, including validation with additional datasets. The results have important implications for the accurate prediction of the three-dimensional interactions of the heel pad with its surroundings and offers valuable insight into the biomechanics of this important structure. To expedite the utility of this model in the field, a download package incorporating optimization and simulation results and the model itself is freely accessible in the 'Downloads' section of the project web site https://simtk.org/home/multidomain.

Acknowledgment

The authors would like to thank Craig Bennetts, MSc, of the Computational Biomodeling (CoBi) Core, Cleveland Clinic, for the reconstruction of three dimensional surface geometry and Pavana Abhiram Sirimamilla, MSc, of the Mechanical and Aerospace Engineering Department, Case Western Reserve University, for contributions to acquisition of mechanical testing data. This study was partially funded by the National Institute of Biomedical Imaging and Bioengineering, National Institutes of Health (Grant No. R01EB006735, Principal Investigator: Antonie J. van den Bogert), in collaboration with Simbios, the NIH Center for Biomedical Computation at Stanford University.

References

[1] De Clercq, D., Aerts, P., and Kunnen, M., 1994, "The Mechanical Characteristics of the Human Heel Pad During Foot Strike in Running: An In Vivo Cineradiographic Study," J. Biomech., **27**(10), pp. 1213–1222.
[2] Rome, K., 1998, "Mechanical Properties of the Heel Pad: Current Theory and Review of the Literature," Foot, **8**(4), pp. 179–185.
[3] Bonanno, D. R., Landorf, K. B., and Menz, H. B., 2011, "Pressure-Relieving Properties of Various Shoe Inserts in Older People With Plantar Heel Pain," Gait and Posture, **33**(3), pp. 385–389.
[4] Sopher, R., Nixon, J., McGinnis, E., and Gefen, A., 2011, "The Influence of Foot Posture, Support Stiffness, Heel Pad Loading and Tissue Mechanical Properties on Biomechanical Factors Associated With a Risk of Heel Ulceration," J. Mech. Behav. Biomed. Mater., **4**(4), pp. 572–582.
[5] Gefen, A., 2010, "The Biomechanics of Heel Ulcers," J. Tissue Viability, **19**(4), pp. 124–131.
[6] Luo, G., Houston, V. L., Garbarini, M. A., Beattie, A. C., and Thongpop, C., 2011, "Finite Element Analysis of Heel Pad With Insoles," J. Biomech., **44**(8), pp. 1559–1565.
[7] Goske, S., Erdemir, A., Petre, M., Budhabhatti, S., and Cavanagh, P. R., 2006, "Reduction of Plantar Heel Pressures: Insole Design Using Finite Element Analysis," J. Biomech., **39**(13), pp. 2363–2370.
[8] Cheung, J. T., and Zhang, M., 2005, "A 3-Dimensional Finite Element Model of the Human Foot and Ankle for Insole Design," Arch. Phys. Med. Rehabil., **86**(2), pp. 353–358.
[9] Cho, J., Park, S., Ryu, S., Kim, S., and Lee, S., 2009, "Landing Impact Analysis of Sports Shoes Using 3-D Coupled Foot-Shoe Finite Element Model," J. Mech. Sci. Technol., **23**(10), pp. 2583–2591.
[10] Chen, W., Lee, T., Lee, P. V., Lee, J. W., and Lee, S., 2010, "Effects of Internal Stress Concentrations in Plantar Soft-Tissue-A Preliminary Three-Dimensional Finite Element Analysis," Med. Eng. Phys., **32**(4), pp. 324–331.
[11] Erdemir, A., Viveiros, M. L., Ulbrecht, J. S., and Cavanagh, P. R., 2006, "An Inverse Finite-Element Model of Heel-Pad Indentation," J. Biomech., **39**(7), pp. 1279–1286.
[12] Gu, Y., Li, J., Ren, X., Lake, M. J., and Zeng, Y., 2010, "Heel Skin Stiffness Effect on the Hind Foot Biomechanics During Heel Strike," Skin Res. Technol., **16**(3), pp. 291–296.
[13] Tao, K., Wang, D., Wang, C., Wang, X., Liu, A., Nester, C. J., and Howard, D., 2009, "An In Vivo Experimental Validation of a Computational Model of Human Foot," J. Bionic Eng., **6**(4), pp. 387–397.
[14] Tong, J., Lim, C. S., and Goh, O. L., 2003, "Technique to Study the Biomechanical Properties of the Human Calcaneal Heel Pad," Foot, **13**(2), pp. 83–91.
[15] Hsu, T. C., Wang, C. L., Shau, Y. W., Tang, F. T., Li, K. L., and Chen, C. Y., 2000, "Altered Heel-Pad Mechanical Properties in Patients With Type 2 Diabetes Mellitus," Diabetic Med., **17**(12), pp. 854–859.
[16] Kinoshita, H., Francis, P. R., Murase, T., Kawai, S., and Ogawa, T., 1996, "The Mechanical Properties of the Heel Pad in Elderly Adults," Eur. J. Appl. Physiol., **73**(5), pp. 404–409.
[17] Lafortune, M. A., and Lake, M. J., 1995, "Human Pendulum Approach to Simulate and Quantify Locomotor Impact Loading," J. Biomech., **28**(9), pp. 1111–1114.
[18] Miller-Young, J. E., Duncan, N. A., and Baroud, G., 2002, "Material Properties of the Human Calcaneal Fat Pad in Compression: Experiment and Theory," J. Biomech., **35**(12), pp. 1523–1531.
[19] Ledoux, W. R., and Blevins, J. J., 2007, "The Compressive Material Properties of the Plantar Soft Tissue," J. Biomech., **40**(13), pp. 2975–2981.
[20] Erdemir, A., Sirimamilla, P. A., Halloran, J. P., and van den Bogert, A. J., 2009, "An Elaborate Data Set Characterizing the Mechanical Response of the Foot," ASME J. Biomech. Eng., **131**(9), p. 094502.
[21] Cavanagh, P. R., 1999, "Plantar Soft Tissue Thickness During Ground Contact in Walking," J. Biomech., **32**(6), pp. 623–628.
[22] *Abaqus 6.7 Theory Manual 2007*, Abaqus, Inc., Pawtucket, RI.

[23] Gefen, A., Megido-Ravid, M., and Itzchak, Y., 2001, "In Vivo Biomechanical Behavior of the Human Heel Pad During the Stance Phase of Gait," J. Biomech., **34**(12), pp. 1661–1665.
[24] Pai, S., and Ledoux, W. R., 2010, "The Compressive Mechanical Properties of Diabetic and Non-Diabetic Plantar Soft Tissue," J. Biomech., **43**(9), pp. 1754–1760.
[25] Petre, M., Erdemir, A., Panoskaltsis, V., Spirka, T., and Cavanagh, P., "Optimization of Nonlinear Hyperelastic Coefficients of Foot Tissues Using an MRI Deformation Experiment," ASME J. Biomech. Eng. (submitted).
[26] Yavuz, M., Tajaddini, A., Botek, G., and Davis, B. L., 2008, "Temporal Characteristics of Plantar Shear Distribution: Relevance to Diabetic Patients," J. Biomech., **41**(3), pp. 556–559.